University of Groningen

On the onset of nano-ordered phase distributions in high-entropy alloys

Rao, J. C.; Ocelík, V.; Vainchtein, D.; Tang, Z.; Liaw, P. K.; De Hosson, J. Th M.

ON THE ONSET OF NANO-ORDERED PHASE DISTRIBUTIONS IN HIGH-ENTROPY ALLOYS

J.C. Rao[1,2], V. Ocelík[2], D. Vainchtein[2], Z. Tang[3], P. K. Liaw[3] and J.Th.M. De Hosson[2]

[1]Institute for Advanced Ceramics, School of Materials Science and Engineering, Harbin Institute of Technology, Harbin 150001, P. R. China
[2]Department of Applied Physics, Zernike Institute for Advanced Materials, University of Groningen, Nijenborgh 4, 9747 AG Groningen, the Netherlands
[3]Department of Materials Science and Engineering, The University of Tennessee, Knoxville, TN 37996, USA

Abstract. This contribution to the Festschrift concentrates on 'nano-s', a topic which is central in Ilya Ovid'ko scientific work in the field of materials physics. In particular, we concentrate on a rather new alloying design concept of so-called High-Entropy Alloys (HEA) that was proposed by Yeh et al. in Adv Eng Mater. 2004;6:299-303. The original idea is that a negative Gibbs free energy of mixing can be achieved, even when the enthalpy of mixing is positive or close to zero, through an increasing mixing entropy contribution with increasing temperature. From theoretical analyses based on the density functional theory, no ordered nanostructures in the Al-Co-Cr-Fe-Ni high-entropy alloys were predicted. However, in contrast ordered *fcc* nanoparticles were discovered by us experimentally in the *fcc* matrix of Al-Co-Cr-Fe-Ni as well as in other systems. In the present paper, we also discovered a novel phenomenon, *i.e.,* the onset of the phase distribution of the *bcc* phase in the *fcc* matrix of $Al_{0.3}CoCrFeNi$. This paper concentrates on the initial stage of locally ordered distribution of bcc phase and reports on the crystallographic orientation relationship between them as $(1\ \text{-}1\ 0)_{bcc}//(200)_{fcc}$, $[001]_{bcc}//[001]_{fcc}$.

1. INTRODUCTION

Since *nanostructures* lie in the focal point of the scientific work of Ilya Ovid'ko, one of the international leaders in this field of research, for this special Festschrift issue of Rev.Adv. Mater.Sci we decided to concentrate on new experimental results in the field of nanostructures in High Entropy Alloys (HEA). A rather new alloy-design concept was proposed in the past by Yeh *et al.* [1-4], in which more than five major elements are combined, with an atomic percentage (at.%) in the range of 5 to 35. The basic idea in developing HEAs is that a negative Gibbs free energy of mixing can be achieved, even when the enthalpy of mixing is positive or close to zero, through an increasing mixing entropy contribution with increasing temperature. Ideally this is so in the case of random solid solution (the so-called regular solution in the quasi-chemical approximation). This trick is often spoiled and hampered by the appearance of intermetallic compounds and the basic idea should be considered as an interesting materials design guideline, not as a 'necessary' and neither as a 'sufficient' condition in materials design.

Many HEAs have been reported to have several promising properties and to be promising materials

---

Corresponding author: J.Th.M. De Hosson, e-mail: j.t.m.de.hosson@rug.nl and J.C. Rao, e-mail: jcrao@hit.edu.cn

for industrial applications [5-7], such as tools, molds, dies, mechanical parts, and furnace parts, which require the high strength, thermal stability, as well as wear and oxidation resistance. The alloys can also be used as anticorrosive high-strength materials in chemical plants, integrated circuit (IC) foundries, and even marine applications for piping components. Research into HEAs addresses their mechanical [8], anticorrosion [9], hydrogen storage [10], and thermophysical properties [11].

The high-entropy effect originates from the significantly higher configurational entropy in HEAs. Such high mixing entropy can favor the formation of disordered solution states and suppress the formation of intermetallic compounds, which is of paramount importance in the application of these alloys [12]. Small atomic-size differences and near-zero values of the absolute enthalpy of mixing facilitate the formation of solid solutions for equiatomic alloys [13,14].

Rather than forming a complex microstructure with a mixture of intermetallic compounds, the idea behind HEAs is to form a simple solid-solution structure, such as face-centered cubic (*fcc*), body-centered cubic (*bcc*), and hexagonal close-packed (*hcp*) structures, or a mixture of them [3,15,16]. It was pointed out that the multi-principal elements high-entropy alloys could easily form simple solid solutions or nano-sized precipitates during solidification due to the high mixing entropy and sluggish cooperative diffusion of substitutional solute atoms [13].

From a materials plasticity viewpoint HEAs are also very interesting and challenging materials because different deformation mechanisms could be clearly detected in the *fcc* and *bcc* phases which is illustrated in Fig. 1 as typical examples of HEAs. Under the same plastic deformation, annealing twins are present only in the *fcc* phase, while the bcc/B2 phases are highly deformed. The *fcc* phase is full of annealing $\Sigma 3$ twins ($60°<111>$), shown in Fig. 1.

Instead of a homogeneous solid solution, nano-scaled phase separation takes place in the single-phase *fcc* HEAs, for example, ordered *fcc* nanoparticles were observed in the *fcc* matrix of $Al_{0.3}CoCrFeNi$ [13,17] and $Al_{0.5}CoCrCuFeNi$ [18]. It was reported that in the $Al_{0.3}CoCrFeNi$ alloy, the $L1_2$ (A1, A2, B2, $L1_2$ etc. are Strukturbericht assignments) structure appears which in fact was considered as an 'ordered solid solution'. It sounds confusing to talk about 'ordered solid solution' but the point is that we are dealing with sub-lattices and the long range order parameter is only exactly equal to 1 for perfect order and perfect stoichiometry. Depending on the occupation probabilities and stoichiometry on the various sub-lattices an 'ordered solid solution' may appear, including short-range ordering. The same accounts for the reported B2 phases which can also be considered as *bcc* in case of equal site occupation probabilities. This trend in HEAs results from the high mixing entropy effect of the multi-principal elements that can effectively decrease the Gibbs free energy of mixing, and, consequently, a solid solution is promoted rather than a fully long-range ordered intermetallic compound during solidification. The sluggish cooperative diffusion effect and the relatively-negative mixing enthalpies between aluminum and other compositional elements can effectively inhibit the growth of phases and promote nanoparticle formation. Criteria of ordered nanoparticle formations are that the Ni con-
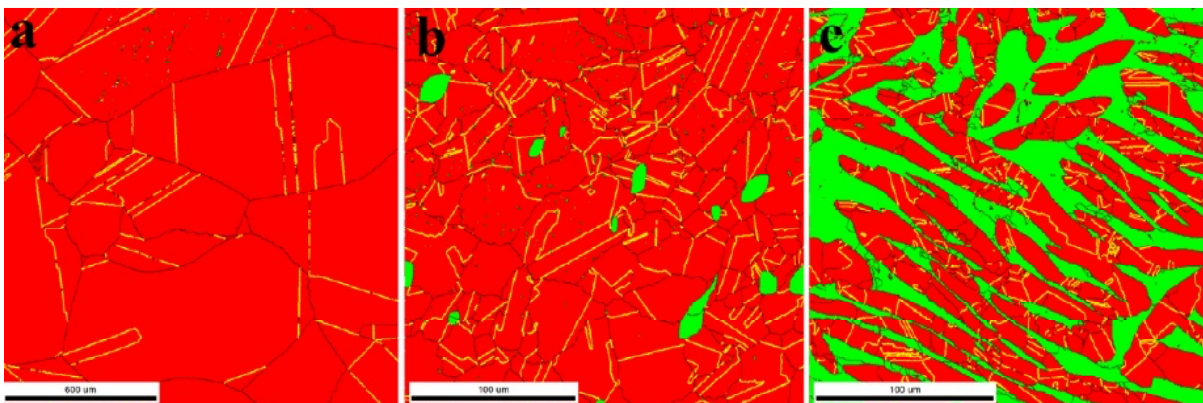

Fig. 1. EBSD phase map of a) Al_0.4, b) Al_0.7 and c) Al_1.0 arc melted samples showing *fcc* (red) and *bcc* (green) phases. Grain boundaries (>5°, black lines) and S3 twin boundaries (yellow lines) in *fcc* phase are also shown.

tent should be larger than 25 atomic percent (at.%) (Ni could be partially substituted by Co) and the aluminum content should be at least 6.25 at.% [18].

2. NANOSTRUCTURED PHASE DISTRIBUTIONS

Ordered versus disordered nanostructures were hardly studied in the field of high-entropy alloys from an experimental viewpoint, neither the case of orientation relationships. In fact only a single publication can be found [19,20]. Theoretically some work has been done on ordering phenomena, e.g. within the framework of the density-functional theory, an electronic-structure-based thermodynamic theory was used to calculate short-ranged order (SRO) in homogeneously-disordered substitutional alloys [21]. The SRO eigenvectors were derived, providing a unique description of the high-temperature SRO in N-component alloys and the low-temperature long-ranged order. This theoretical analysis was applied to ternary alloys (A1 Cu-Ni-Zn and A2 Nb-Al-Ti) for validation, and then to quintenary Al-Co-Cr-Fe-Ni high-entropy alloys for the predictive assessment]21]. SRO was investigated in Al-Co-Cr-Fe-Ni systems in three regions with different aluminum content, that is, Al poor with mole fraction, $\Delta < 0.5$, Al intermediate with $0.5 \leq \Delta \leq 1.25$, and Al rich with $1.25 < \Delta \leq 2.0$, all of which show only simple solid-solution phases, i.e., A1, A2, or both [22].

From this theoretical evaluation, ordered structures in the Al-Co-Cr-Fe-Ni high-entropy alloys cannot exist, although the calculation cannot exactly tell us what the microstructure will be. Despite the recent advances in computational materials science, we have to wait until it becomes fully realized. Nevertheless, ordered *fcc* nanoparticles were discovered experimentally in the *fcc* matrix in Al-Co-Cr-Fe-Ni before [13,18,22] but in the present work, we discovered a novel phenomenon, namely the onset of an ordered distribution of the *bcc* phase in the *fcc* matrix of $Al_{0.3}CoCrFeNi$. The morphology and the crystallographic orientation relationship between them were studied in detail.

3. EXPERIMENTAL OBSERVATIONS AND ANALYSIS

Ingots with the nominal composition of the $Al_{0.3}CoCrFeNi$ alloy was prepared by arc-melting pure elements with a purity higher than 99.95 weight percent under a high-purity argon atmosphere on a water-cooled Cu hearth. The alloy was re-melted four times in order to obtain homogeneity [19,20,22].

Then it was homogenized at 1250 °C for 50 h after casting. Several thin foils for transmission electron microscope (TEM) observation were prepared from the middle of the bulk materials by conventional mechanical grinding and polishing with SiC-abrasive papers gradually and finished by ion milling at 4 kV in a PIPS 691 system (Gatan, Inc., Pleasanton, CA, USA). A JEM 2010F transmission electron microscope (JEOL Ltd., Tokyo, Japan), operating at 200 kV, equipped with an energy dispersive x-ray spectroscopy (EDS) system (127 eV resolution, Bruker Corporation, Billerica, MA, USA), was used for the selected area-electron-diffraction (SAED) analysis and high-resolution TEM (HRTEM) observations. JEM 4000 EXII TEM (JEOL Ltd., Tokyo, Japan) was also used for the HRTEM observation operating at 400 kV. The high-resolution images were recorded around Scherzer defocus, i.e., - 43 nm for the microscopes of JEM 2010F and - 51 nm for JEM 4000 EXII therein used, respectively. Fast Fourier transformation (FFT) was carried out using a DigitalMicrograph software package (Gatan, Inc. USA).

The phase constitution in the $Al_{0.3}CoCrFeNi$ sample appears to be a single solid solution *fcc* phase (face-centered cubic, an A1 structure) by X-Ray Diffraction (XRD). Twins were visible in scanning electron microscope (SEM), while no segregation was observed. The mean grain size is about 500 μm.

Table 1 summarizes the data of the Electron-Back Scattering Diffraction (EBSD) results of phase, grain size, and twins in $Al_{0.3}CoCrFeNi$ comparing with $Al_{0.5}CoCrFeNi$ and $Al_{0.7}CoCrFeNi$ alloys (see also Fig. 1). In contrast, our detailed TEM analysis confirms that there are not only *fcc* phases, but also *bcc* phases to some content, which are homogeneously distributed on a nano-scale with a basic crystallographic-orientation relationship between these two phases in the $Al_{0.3}CoCrFeNi$ alloy. The volume fraction of the *bcc* phase is far less than that of the *fcc* phase. The EDS results from the different areas of the same grain with a 1-nm electron-beam size prove that the material is homogeneous. The chemical composition is close to the formula of $Al_{0.3}CoCrFeNi$. While the selected area-electron-diffraction patterns indicate there are at least two sets of patterns for different phases instead of pure *fcc* phase, as shown in Fig. 2.

Fig. 2a is the TEM bright field (BF) micrograph showing dislocations clearly. The basic crystallographic orientation relationship between the *bcc* and *fcc* phases are denoted clearly in Fig. 2b as $(1\ \text{-}1\ 0)_{bcc}//(200)_{fcc}$, $[001]_{bcc}//[001]_{fcc}$. The dark-field (DF)

Table 1. EBSD results of phase, grain size, and twins in $Al_{0.3}CoCrFeNi$, $Al_{0.5}CoCrFeNi$ and $Al_{0.7}CoCrFeNi$ alloys.

Alloy	Phases [%]		Grain size [mm]		Twinned *fcc* grains[%]		
Parameter/Material	*fcc*	*bcc*	*fcc*	*bcc*	Untwinned	Parent	Daughter
$Al_{0.3}CoCrFeNi$	99.9	0.1	500	-	9.6	50.9	39.5
$Al_{0.5}CoCrFeNi$	96.9	3.1	40.3	11.9	1.8	59.9	38.3
$Al_{0.7}CoCrFeNi$	65.2	34.8	23.2	27.9	9.1	48.8	42.1

image with a DF1 spot [(1 -1 0) spot of the *bcc* phase] in Fig. 2c shows that the *bcc* phases are continuous when being observed at lower magnification, while the DF image with the DF2 spot [(200) spot of the *fcc* phase] in Fig. 2d indicates that the *fcc* phases are also continuous but with both coarse and fine structures in the whole grain, except for thickness and bending contours. The dark network refers to the *bcc* phase.

The HRTEM images also supported the aforementioned conclusion, as shown in Fig. 3. Fig. 3a gives a HRTEM micrograph taken in JEM 2010F at 200 kV. It is shown that the main *fcc* phase is continuous, while the *bcc* phase is mutually interpenetrated with the *fcc* phase. The FFT result in Fig. 3b shows that there are both *fcc* and *bcc* phases with the aforementioned orientation relationship. Dislocations are clearly visible in the *bcc* phase but

fewer in the *fcc* phase as presented clearly by the inverse FFT micrographs in Figs. 3c and 3d for *fcc* and *bcc* phases, respectively. These dislocations are important for the mismatch between the {200} planes of the *fcc* phase and the {1 -1 0} planes of the *bcc* phase.

Fig. 4 shows a HRTEM micrograph as well as the electron diffraction pattern (EDP) and its FFT results taken from the JEM 4000EXII at 400 kV. A modulated structure is observed in Fig. 4a. The recorded corresponding EDP in Fig. 4b indicates that both the *fcc* and the *bcc* structures are present, with an orientation relationship in the [001] direction, as depicted in Fig. 3. The FFT result of the HRTEM image in Fig. 4c matches the recorded EDP
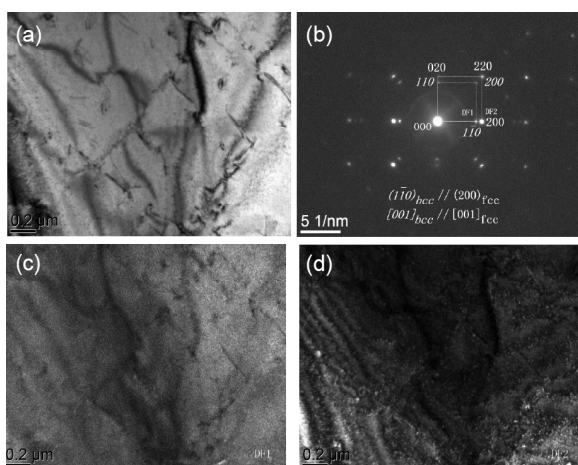

Fig. 2. TEM micrographs of $Al_{0.3}CoCrFeNi$ at room temperature (a) BF image, (b) EDP showing the orientation relationship between the *bcc* and the *fcc* phases of $(1 -1 0)_{bcc}//(200)_{fcc}$ and $[001]_{bcc}//[001]_{fcc}$, (c) DF image with (1 -1 0) spot of the *bcc* phase, and (d) DF image with the (200) spot of the *fcc* phase.
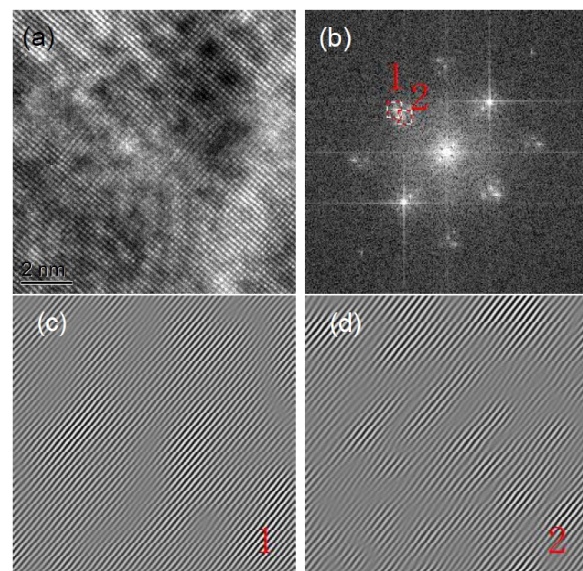

Fig. 3. HRTEM micrograph and FFT and IFFT results (a) HRTEM image along the [001] direction of both the *fcc* and the *bcc* phases by JEM 2010F at 200 kV, (b) FFT result, (c) IFFT result with the (200) spot of the *fcc* phase, and (d) IFFT result with the (1 -1 0) spot of the *bcc* phase.
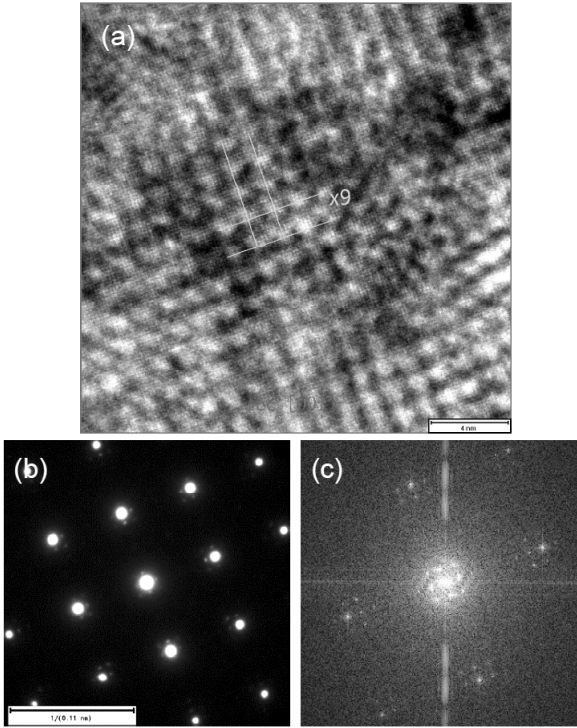
Fig. 4. HRTEM micrograph as well as the corresponding EDP and its FFT results of the *fcc* phase by JEM 4000EXII at 400 kV (a) HRTEM micrograph showing the modulated structure, (b) the EDP for HETEM in the [001] direction of both the *fcc* and the *bcc* phases, and (c) FFT result of the HRTEM image, which matches the recorded EDP very well.
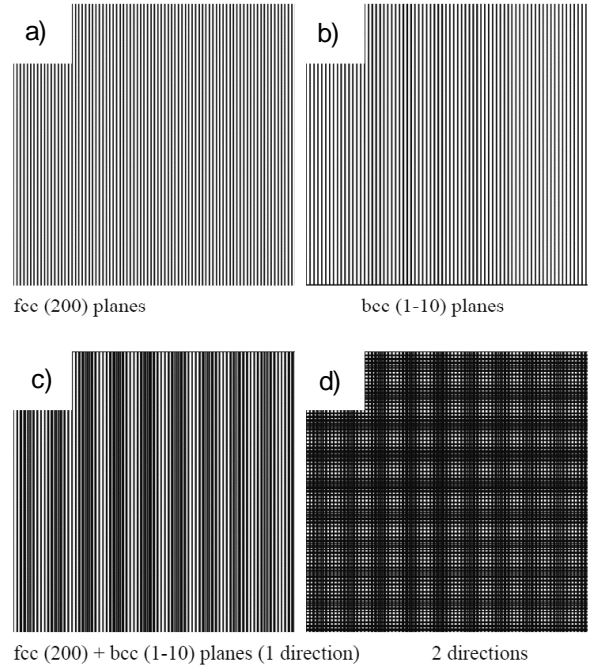

Fig. 5. Moiré fringe simulations (a) (200) planes of the *fcc* phase in the [001] direction, (b) (1 -1 0) planes of the *bcc* phase in the [001] direction, (c) overlapping in one direction with $(1\text{ -}1\text{ }0)_{bcc}//(200)_{fcc}$, and (d) overlapping in two perpendicular directions.

very well and indicates that at least this area is rather free of defects.

The parameters of the *fcc* and the *bcc* phases are a_{fcc} = 0.36009 nm, and a_{bcc} = 0.28786 nm, respectively, as revealed also by XRD. According to the orientation relationship $[(1\text{-}10)_{bcc}//(200)_{fcc}$, $[001]_{bcc}//[001]_{fcc}]$ obtained by the EDPs shown above, the fringes of planes in the *fcc* and the *bcc* phases can be drawn out as shown in Fig. 5.

The period, p, of moiré fringes or patterns can be calculated using [23]:

$$p_m = \frac{p_b \cdot p_r}{p_b - p_r},$$

where p_b and p_r are the periods of base and revealing layers, or simply say of layers 1 and 2. The interplanar distances are $(200)_{fcc}$ = 0.1800 nm and $(1\text{ -}1\text{ }0)_{bcc}$ = 0.2035 nm, respectively. Then p_m = 1.5587 nm. This value equals to 9 times of $(200)_{fcc}$ and 8 times of $(1\text{ -}1\text{ }0)_{bcc}$ and this trend matches the observations in the HRTEM images. The simulated moiré fringes both in one and two directions are

clearly seen, and the recorded HRTEM images can be matched.

Fig. 4 shows the simulation results of moiré fringes. Solid lines in Figs. 5a and 5b indicate the {200} planes of the *fcc* and the {1 -1 0} planes of the *bcc* phases in the same [001] direction, respectively. The overlap is given in Fig. 5c in one direction with $(1\text{ -}1\text{ }0)_{bcc}//(200)_{fcc}$, while Fig. 5d shows the overlap in two perpendicular directions. The simulated results agree very well with the experimental images.

It should be noted that the *bcc* phase is thinly and homogeneously distributed in all over the grain as well as the *fcc* phase, although some crystallites of the *fcc* phase coarsened, as shown in BF and DF images in Fig. 2. When the selected area-electron-diffraction pattern was recorded, the *bcc* phase cannot be effectively excluded. The HRTEM image becomes modulated locally both due to the *fcc* and the *bcc* phases as well as the diffraction patterns by dynamic effect, like double diffraction. It is well known that a slight change in composition

would form other phases in the alloy systems. But it is very interesting that the newly formed *bcc* phase is trying to keep strict crystallographic orientation relationship with *fcc* matrix even on a nano-scale. It is very difficult to discern these two phases in the morphology.

4. CONCLUSIONS

In summary: in high-entropy alloy like $Al_{0.3}CoCrFeNi$ both the *fcc* and the *bcc* phase are present, homogeneously distributed on a nano-scale with a basic crystallographic orientation relationship of $(1 \text{-}1\ 0)_{bcc}/ /(200)_{fcc}$, $[001]_{bcc}//[001]_{fcc}$. These nano-scaled phases can be regarded as the initial stage of ordered distribution of the *bcc* phase in the *fcc* matrix of Al-Co-Cr-Fe-Ni high-entropy alloys. These abundant amounts of multi-elemental ordering-distributed nanostructures with the special orientation relationship with the matrix can be considered to contribute to the excellent physical and mechanical properties of high-entropy alloys.

Clearly a novel integrated approach is needed, i.e. combining in-situ TEM observation, Atom Probe Tomography, EBSD, neutron diffraction, and detailed thermodynamic calculations as the next step to deepen our fundamental understanding on the phase stability and plastic deformation mechanisms of both single-phase and multi-phase HEAs at elevated temperatures through the integration of experimental and theoretical approaches [24].

ACKNOWLEDGEMENTS

REFERENCES

[1] J.W. Yeh, S.K. Chen, S.J. Lin, J.Y. Gan, T.S. Chin and T.T. Shun // *Adv. Eng. Mater.* **6** (2004) 299.

[2] M.H. Chuang, M.H. Tsai, W.R. Wang, S.J. Lin and J.W. Yeh // Acta Mater. **59** (2011) 6308.

[3] Y. Zhang, T.T. Zuo, Z. Tang, M.C. Gao, K.A. Dahmen and P.K. Liaw // *Prog. Mater. Sci.* **61** (2014) 1.

[4] J.W. Yeh // *Ann. Chim. – Sci. Mater.* **31** (2006) 633.

[5] C.Y. Hsu, C.C. Juan, S.T. Chen, T.S. Sheu, J.W. Yeh and S.K. Chen // *JOM* **65** (2013) 1829.

[6] Y.Y. Chen, T. Duval, U.D. Hung, J.W. Yeh and H.C. Shih // *Corros. Sci.* **47** (2005) 2257.

[7] O.N. Senkov, G.B. Wilks, D.B. Miracle, C.P. Chuang and P.K. Liaw // *Intermetallics* **18** (2010) 1758.

[8] Y.F. Kao, T.J. Chen, S.K. Chen and J.W. Yeh // *J. Alloys Compd.* **488** (2009) 57.

[9] Y.F. Kao, T.D. Lee, S.K. Chen and Y.S. Chang // *Corros. Sci.* **52** (2010) 1026.

[10] Y.F. Kao, S.K. Chen, J.H. Sheu, J.T. Lin, W.E. Lin and J.W. Yeh // *Int. J. Hydrogen Energy* **35** (2010) 9046.

[11] H.P. Chou, Y.S. Chan, S.K. Chen and J.W. Yeh // *Mater. Sci. Eng. B.* **163** (2009) 184.

[12] C.J. Tong, Y.L. Chen, S.K. Chen, J.W. Yeh, T.T. Shun and C.H. Tsau // *Metall Mater. Trans. A* **36** (2005) 881.

[13] Y. Zhang, Y.J. Zhou, J.P. Lin, G.L. Chen P.K. Liaw // *Adv. Eng. Mater.* **10** (2008) 534.

[14] S. Singh, N. Wanderka, B.S. Murty, U. Glatzel and J. Banhart // *Acta Mater.* **59** (2011) 182.

[15] M. Feuerbachera, M. Heidelmanna and C. Thomas // *Materials Research Letters* **3** (2015) 1.

[16] K.M. Youssef, A.J. Zaddach, C.N. Niu, D.L. Irving and C.C. Koch // *Materials Research Letters* **3** (2015) 95.

[17] T.T. Shun, C.H. Hung and C.F. Lee // *J Alloys Compd.* **493** (2010) 105.

[18] X.D. Xu, P. Liu, S. Guo, A. Hirata, T. Fujita and T.G. Nieh // *Acta Mater.* **84** (2015) 145.

[19] J.C. Rao, V. Ocelík, D. Vainchtein, Z. Tang, P.K. Liaw amd J.Th.M. De Hosson // *Materials Letters* **176** (2016) 29, http://dx.doi.org/10.1016/j.matlet.2016.04.086.

[20] V. Ocelik, N. Janssen, S.N. Smith and J.Th.M. De Hosson // *J. of Metals* **68** (2016) 1810, http://dx.doi.org/10.1007/s11837-016-1888-z.

[21] P. Singh, A.V. Smirnov and D.D. Johnson // *Phys Rev B.* **91** (2015) 224204.

[22] S.G. Ma, P.K. Liaw, M.C. Gao, J.W. Qiao, Z.H. Wang and Y. Zhang // *J. Alloys Compd.* **604** (2014) 331.

[23] B. Fultz and J. Howe, *Transmission electron microscopy and diffractometry of materials*, Fourth ed. (Springer-Verlag, Berlin Heidelberg, 2013).

[24] J. C. Rao , H. Y. Diao, V. Ocelík, D. Vainchtein, C. Zhang , C. Kuo, Z. Tang , W. Guo, J. D. Poplawsky, Y. Zhou, P. K. Liaw and J. Th. M. De Hosson, *Secondary phases in AlxCoCrFeNi high-entropy alloys: an in-situ TEM heating study and thermodynamic appraisal,* in preparation (2017).